Environ. Sci. Technol. 2002, 36, 5469–5475

Formation of Ferrihydrite and Associated Iron Corrosion Products in Permeable Reactive Barriers of Zero-Valent Iron

YOKO FURUKAWA,*,† JIN-WOOK KIM,† JANET WATKINS,† AND RICHARD T. WILKIN‡

Naval Research Laboratory, Seafloor Sciences Branch, Code 7431, Stennis Space Center, Mississippi 39529, and U.S. Environmental Protection Agency, Office of Research and Development, National Risk Management Research Laboratory, Ada, Oklahoma 74820

Ferrihydrite, which is known to form in the presence of oxygen and to be stabilized by the adsorption of Si, PO_4 and SO_4, is ubiquitous in the fine-grained fractions of permeable reactive barrier (PRB) samples from the U.S. Coast Guard Support Center (Elizabeth City, NC) and the Denver Federal Center (Lakewood, CO) studied by high-resolution transmission electron microscopy and selected area electron diffraction. The concurrent energy-dispersive X-ray data indicate a strong association between ferrihydrite and metals such as Si, Ca, and Cr. Magnetite, green rust 1, aragonite, calcite, mackinawite, greigite and lepidocrocite were also present, indicative of a geochemical environment that is temporally and spatially heterogeneous. Whereas magnetite, which is known to form due to anaerobic Fe^0 corrosion, passivates the Fe^0 surface, ferrihydrite precipitation occurs away from the immediate Fe^0 surface, forming small (<0.1 μm) discrete clusters. Consequently, Fe^0-PRBs may remain effective for a longer period of time in slightly oxidized groundwater systems where ferrihydrite formation occurs compared to oxygen-depleted systems where magnetite passivation occurs. The ubiquitous presence of ferrihydrite suggests that the use of Fe^0-PRBs may be extended to applications that require contaminant adsorption rather than, or in addition to, redox-promoted contaminant degradation.

Introduction

Permeable reactive barriers (PRBs) of zero-valent iron (Fe^0) filings have proven to be a promising technology for the remediation of groundwater containing contaminants such as hexavalent chromium, uranium, and nitroaromatic compounds (*1–8*). Iron corrosion processes and subsequent authigenic mineral precipitation have become concerns for the long-term performance of Fe^0-PRBs yet few data are available that address the consequences of long-term corrosion to remedial performance (*9*). Iron corrosion in an Fe^0-PRB by groundwater is initiated by

$$Fe^0 + \frac{1}{2}O_2 + H_2O \rightarrow Fe^{2+} + 2OH^- \qquad (I)$$

in oxic environments, or by

$$Fe^0 + 2H_2O \rightarrow Fe^{2+} + H_2 + 2OH^- \qquad (II)$$

in anoxic environments. Previous laboratory and field studies have shown the development of surface corrosion and authigenic precipitates (*1, 3, 9–13*). Such surface precipitates may mask the redox-active sites where exchange of electrons between Fe^0 and contaminants is facilitated. The corrosion products may also reduce the barrier permeability by occupying available pore space. On the other hand, the formation of iron oxyhydroxides with large surface areas may be beneficial for the immobilization of certain contaminants (e.g., arsenic) through sorption or coprecipitation (*14, 15*).

Several recent studies reported the identity of authigenic phases in field-deployed and laboratory-simulated Fe^0-PRBs. Authigenic phases recovered from field installations studied by Roh et al. (*16*) include amorphous iron hydroxides, green rust minerals, goethite, aragonite, calcite, siderite, mackinawite and elemental sulfur.

Phillips et al. (*12*) investigated the authigenic precipitates at the Oak Ridge Y-12 site and found crystalline ferric oxyhydroxides, aragonite, siderite and amorphous FeS. Experiments in a laboratory flow-through system yielded lepidocrocite, akaganeite, mackinawite, magnetite, maghemite, goethite, siderite, green rusts, and amorphous FeS (*12, 13*). These phases were determined through X-ray powder diffraction (XRD) analysis of the fine-grained fractions separated by sonication. Some phases such as amorphous FeS and green rusts were inferred from the combined data of crystal habit (by scanning electron microscopy, SEM) and elemental compositions (by energy-dispersive X-ray analysis, EDX) because XRD does not allow a positive identification of amorphous phases or a phase consisting of a minor weight fraction of the total sample mass (*16*).

These previous studies of Fe^0-PRBs have described the primary corrosion products in their respective environments of formation. However, the techniques employed, i.e., combination of XRD, EDX and morphology observations, do not permit complete identifications of poorly crystallized phases that may play a significant role in contaminant adsorption and authigenic paragenesis.

This study utilizes high-resolution transmission electron microscopy (HRTEM) and EDX to simultaneously analyze the phase assemblages, morphology and spatial relationships among the authigenic precipitates of Fe^0-PRBs. In particular, this study takes advantage of selected area electron diffraction (SAED) to identify the mineral phases that may not be recognized by XRD due to their insufficient quantities or poor crystallinity.

Experimental Section

Materials. The samples were collected in the summer of 2000 from two PRBs installed in 1996 at the U.S. Coast Guard Support Center (Elizabeth City, NC) and Denver Federal Center (Lakewood, CO). The hydrogeology and barrier configurations of the sites are described elsewhere (*1, 9, 16*). The Elizabeth City (EC) barrier is a continuous wall, whereas the Denver Federal Center (DFC) barrier has a funnel-and-gate configuration. The sample collection and analytical procedures for the groundwater chemistry determination are described in ref *9*. The results (Table 1) show that the groundwater chemistry changes due to interactions with Fe^0

* Corresponding author phone: (228)688-5474; fax: (228)688-5752; e-mail: yoko.furukawa@nrlssc.navy.mil.
† Naval Research Laboratory.
‡ U.S. Environmental Protection Agency.

10.1021/es025533h Not subject to U.S. Copyright. Publ. 2002 Am. Chem. Soc. Published on Web 11/13/2002

TABLE 1. Summary of Groundwater Chemistry at Elizabeth City (June 2000) and Denver Federal Center (July 2000) from Ref 9[a]

	Elizabeth City		Denver – gate 1		Denver – gate 2	
	aquifer	barrier	aquifer	barrier	aquifer	barrier
pH	5.94	9.51	7.24	10.30	7.80	9.90
Eh (mV)	491	−347	233	−247	281	−35
O_2 (mg/L)	0.3	0.1	0.92	0.1	0.3	0.1
H_2 (nM)	N/A	N/A	0.63	949	2.38	304
Na (mg/L)	50	29	179	194	167	249
K (mg/L)	3.0	3.1	0.39	0.6	0.27	0.95
Mg (mg/L)	9.1	3.2	18.1	3.9	31	61
Ca (mg/L)	16.4	5.3	100	1.2	114	4.1
Fe (mg/L)	<0.04	0.05	0.19	<0.04	<0.04	<0.04
SO4 (mg/L)	49	<1.0	234	<1.0	296	359
Cl (mg/L)	51	25	52	59.7	66	83
NO3 (mg/L)	0.9	<0.1	3.2	<0.1	2.9	1.1
Si (mg/L)	10.9	<0.2	13.2	0.3	14.8	0.3
DIC (mg/L)	15	8	86	60	95	46
DOC (mg/L)	1.2	0.9	2.3	1.8	1.6	3.3
TDS (mg/L)	290	143	1090	510	1172	1011

[a] DIC, dissolved inorganic carbon; DOC, dissolved organic carbon; TDS, total dissolved solid.

as indicated by the pH increase, Eh decrease, Ca, Mg and Si concentration decrease, and dissolved inorganic carbon (DIC) decrease. The sampling schemes for authigenic phase analysis reported in this paper are described in ref 9. Briefly, 5 cm i.d. cores were collected from immediately inside the reactive barriers at the upgradient portions in the regions of maximum authigenic phase accumulations, as well as from mid-barrier regions. The samples for authigenic phase mineralogy were stored in N_2 until the time of examination by HRTEM, SAED and EDX. A portion of the sample from EC site was sonicated in acetone to mechanically separate fine-grained precipitates from coarse Fe^0 filings prior to storage. The bulk EC samples were also impregnated in resin, polished, and examined with SEM. The fine-grained fraction from EC, separated by sonication, was analyzed by XRD. SEM observations of this separated fraction confirmed the particle size to be 10 μm or smaller. Seventy-one cores from EC and DFC were analyzed for microbial assays (PLFA) as described in ref 9.

Transmission Electron Microscopy. The bulk samples from EC and DFC, and the sonicated fine-grained fraction (~< 10 μm) from EC, were shaken onto amorphous carbon film supported by copper grids. Excess materials were removed from the film by gentle tapping. Only the very small (< several μm) particles and aggregates remained on the grids due to static charge, whereas larger particles were eliminated. Consequently, the observations were made on fine-grained precipitates that were not attached to the surface of original coarse Fe^0 filings either by physical or chemical means, rather than on the precipitates that were firmly bound to the Fe^0 surfaces.

The samples were observed using the bright-field imaging mode of JEOL 3010 TEM with an acceleration voltage of 300 keV at magnifications from 40 000x to 400 000x. The images were accompanied by EDX spectra collected with Noran EDX detector using an electron beam diameter of approximately 700 nm and by SAED patterns generated using a 500 nm diameter area-selecting aperture.

The EDX data were used to identify the elements present. Because the samples were placed on carbon film supported by copper grids, the EDX spectra always contained signals from Cu and C.

The SAED ring patterns were recorded on film and analyzed for their diameters, which were converted to d-spacing values. The values were then compared against the known d-spacing values of hematite, maghemite, magnetite, lepidocrocite, goethite, akaganeite, siderite, calcite, aragonite, mackinawite, greigite, pyrite (from JCPDS cards), green rust minerals (*17–19*), 2-line ferrihydrite (*20*), and 6-line ferrihydrite (*20*).

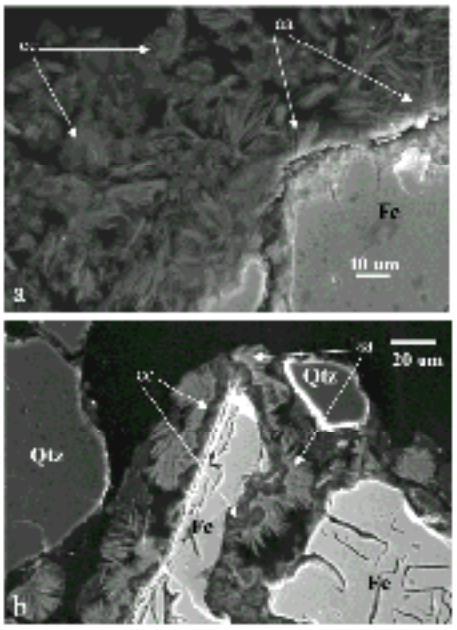

FIGURE 1. SEM images of an embedded and polished sample from EC showing the spatial relationships between Fe^0 filings (Fe), acicular aggregates (aa), and cryptocrystalline clusters (cc). Some quartz grains (Qtz) from the native aquifer materials are also present.

Whereas SAED is an appropriate technique for identifying crystalline phases existing as single-phase aggregates or occupying large fractions of multiphase aggregates, it cannot identify phases that are not in aggregates or are minor components of aggregates. Thus, lattice fringe images were used to assist the phase identification when appropriate.

Results and Discussion

SEM and XRD Observations. SEM images of the EC samples (Figure 1) exhibit two types of authigenic precipitate morphology: acicular aggregates and cryptocrystalline clusters. Individual needles in the acicular aggregates are up to approximately 10 μm long, whereas the size of each cryptocrystalline cluster cannot be discerned with the resolution of these images. The observed morphologies are consistent with the previous SEM results (*10–13*). Previous studies showed that acicular aggregates were largely composed of green rust minerals, goethite, lepidocrocite, and calcium carbonate phases, whereas cryptocrystalline clusters contained mackinawite and poorly crystallized iron (oxy-) hydroxides.

XRD data from the EC fine-grained fraction are shown with all major peak positions and relative intensities for magnetite and mackinawite (from JCPDS) and carbonate green rust (from ref *19*) as well as three major peak positions and relative intensities for calcite, aragonite, siderite, goethite and lepidocrocite (from JCPDS) (Figure 2). XRD data indicate that the EC upgradient interface, which is in continuous contact with untreated groundwater, contains magnetite, carbonate green rust, mackinawite, lepidocrocite, calcite and aragonite. Siderite was not detected. The sample from mid-barrier region lacks lepidocrocite and mackinawite.

The precipitation of calcium carbonate phases at the EC upgradient interface can be described in the stability diagram (Figure 3). The groundwater originally undersaturated with respect to aragonite experiences a steep increase in pH upon entering the barrier due to Fe^0 oxidation (reactions I and II

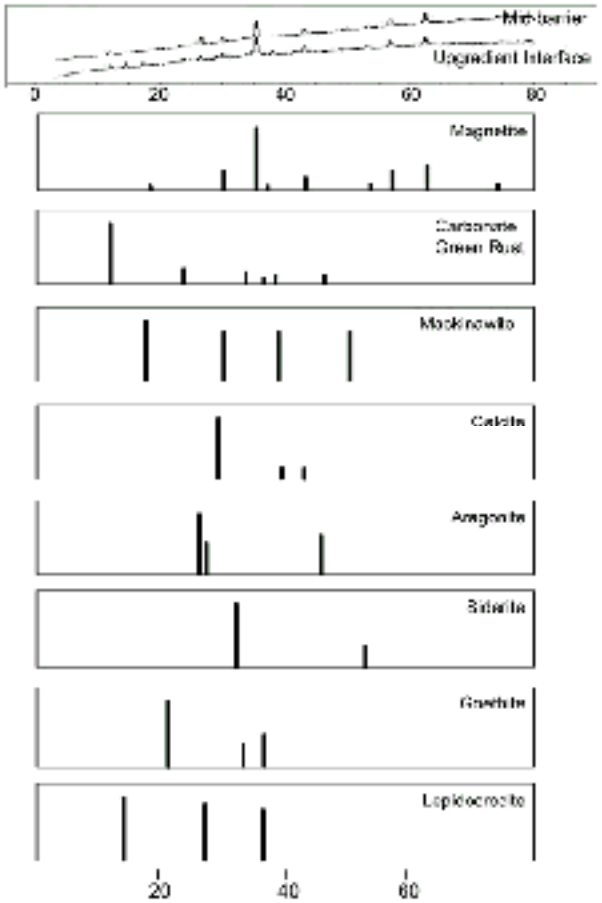

FIGURE 2. X-ray diffractograms of EC samples from near the upgradient boundary and in mid-barrier, shown with the indexing peaks of selected phases. Peaks for magnetite, carbonate green rust, lepidocrocite, mackinawite, and calcium carbonate phases are observed.

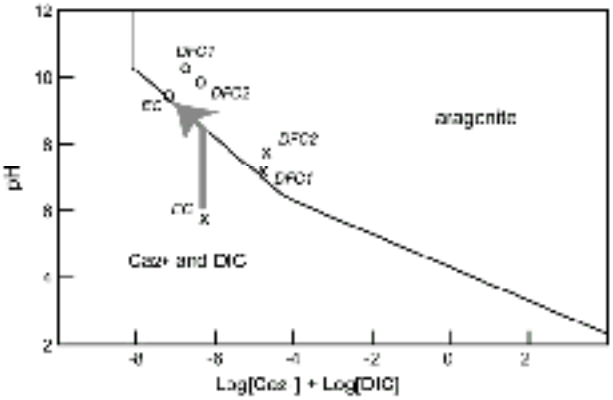

FIGURE 3. Aragonite stability field is indicated as a function of pH and *Log* concentrations of Ca^{2+} and DIC. The groundwater compositions of unreacted aquifer (x) and mid-barrier water (O) are also plotted for Elizabeth City (EC), Denver Federal Center Gate-1 (DFC1), and Gate-2 (DFC2). The changes in EC groundwater composition upon entering the barrier are shown by the gray arrow. above), and precipitates aragonite. The majority of Ca^{2+} and DIC may be removed in the vicinity of upgradient interface as aragonite. Subsequently, the Ca^{2+} and DIC concentrations and pH become regulated by continuing aragonite precipitation, while groundwater passes through the reactive media with further addition of OH^-. The DFC groundwater, which is high in total dissolved solids, is buffered by calcium carbonate prior to the barrier entry and its chemistry is fixed along the carbonate mineral stability boundary during travel through the barrier (Figure 3). The negative effect of calcium carbonate precipitates (i.e., decreasing permeability, Fe^0 surface coating) is expected to be most pronounced at the upgradient interface regions of PRBs.

TEM Observations. TEM bright field images of EC samples prepared from both bulk samples and sonicated fine-grained fraction exhibit cryptocrystalline clusters as well as large (>500 nm long) elongated crystals (Figure 4). The elongated crystals are always closely associated with the cryptocrystalline clusters (e.g., Figure 4a,g). Cryptocrystalline clusters are composed of numerous small (<50 nm), rounded to polyhedral grains and small number of acicular particles of 50−200 nm long (e.g., Figure 4d). The cryptocrystalline clusters observed under TEM are most likely the component of the cryptocrystalline clusters observed under SEM. The acicular aggregates seen in the SEM images are probably composed of the elongated crystals seen under TEM.

SAED patterns of the cryptocrystalline clusters from EC show diffuse diffraction rings corresponding to the d-spacing values of 0.25 and 0.15 nm, that are characteristic ferrihydrite reflections (*20*) (Figure 4c,e). The ferrihydrite rings are often overlaid with the well-defined diffraction rings of magnetite (Figure 4e). Ferrihydrite is a poorly crystallized, fine-grained iron hydroxide often found as a byproduct of hydrometallurgical processing and as a product of steel corrosion (*22*). In nature, it occurs in rapidly weathered iron-rich soils, especially in soils that contain dissolved silica, phosphate or other ions that are sorbed on the ferrihydrite surfaces to inhibit conversion to more crystalline assemblages, and in soils that experience oscillating redox environments (*23, 24*). Its large specific surface area and unsaturated surface coordination make it an environmentally valuable mineral (*22*). The EDX spectrum of the cryptocrystalline cluster (Figure 4f) indicates that the cluster has incorporated chromium, the primary contaminant at the EC site.

SAED and EDX analyses were conducted on a total of 35 cryptocrystalline clusters from EC (Table 2). The most common phase assemblage found by SAED was magnetite plus ferrihydrite. Ferrihydrite was nearly ubiquitous, while SAED occasionally identified other phases such as goethite, hematite, siderite, mackinawite, greigite, and pyrite. The abundance of ferrihydrite observed in this study contrasts with previous studies in which ferrihydrite was largely unmentioned (*10−13*). This is probably because phase identifications in previous studies were carried out through XRD that is not suitable for poorly crystallized phases due to the low, wide diffraction peaks that may not be distinguishable from background. For the same reason, ferrihydrite was not detected through XRD in this study (e.g., Figure 2).

In addition to Fe, EDX detected Si, Cr, and Ca in many of the cryptocrystalline clusters with occasional Mn (Table 2). Whereas the EDX data do not single out ferrihydrite as the only important phase for metal adsorption, they do positively indicate the association between ferrihydrite and metals: all six of the ferrihydrite-only clusters contain Si, whereas a large fraction of them also contain Ca, Cr, and Mn. The EC groundwater chemistry data (Table 1) suggest that the PRB is a sink for both Ca and Si. Ferrihydrite is known to strongly adsorb Si, which stabilizes ferrihydrite and retards the further oxidation to ferric oxyhydroxides (*27−30*). Field observations have shown that Fe^0-PRBs are long-term sinks for dissolved Si from groundwater (*9*). It has been previously shown that the sorption of Mn(VI), Cr(III), Ca(II), and SO_4^{2-} onto ferrihydrite surfaces also occurs (*31−34*), which is consistent with the observed EDX spectra.

A high magnification image of the outlined portion of Figure 4a gives lattice fringes with 0.6 nm spacing (Figure 4b). Many of the elongated crystals are identified as lepidocrocite from their crystal habit as well as this characteristic lattice fringe spacing that corresponds to lepidocrocite (020)

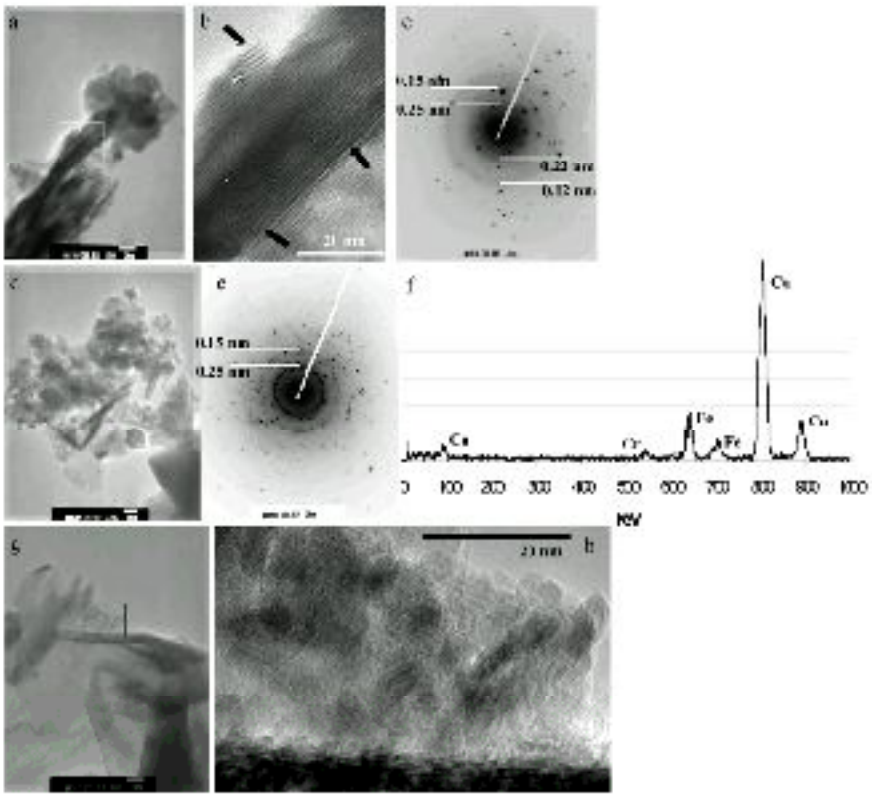

FIGURE 4. TEM results from BC samples: (a) an elongated crystal closely associated with a rounded cluster of small (<40 nm) particles; (b) magnified image of a portion of (a) (rectangle enclosure) exhibiting several well-defined lattice fringes (arrows) with the value of 0.6 nm, which corresponds to the lepidocrocite (020) (*27*); (c) SAED image of the rounded cluster in (a), revealing diffuse diffraction rings that correspond to the *d*-spacing values of 0.25 and 0.15 nm, typical of ferrihydrite (*20*), together with the diffraction rings from amorphous carbon film (sample holder) at 0.22 and 0.12 nm and strong diffraction spots from the adjacent elongated lepidocrocite; (d) a cluster of small (<50 nm) rounded particles and small (<200 nm long) acicular particles; (e) SAED image of the cluster in (d) exhibiting diffuse diffraction rings from ferrihydrite at 0.25 and 0.15 nm overlaid with the darker, better defined diffraction rings and spots of magnetite; (f) EDX spectrum from the cluster in (d) indicating the presence of Cr and Fe (Cu signals are from the sample holder); (g) an area containing both elongated crystals and cryptocrystalline clusters; (h) the magnified image of a cryptocrystalline cluster in (g) (rectangle box) revealing domains of nearly uniform size (~5−10 nm).

TABLE 2. SAED-Based Phase Assemblages and EDX-Based Minor Element Inventory for BC Cryptocrystalline Clusters[a]

phase assemblage by SAED								no. of clusters	Cr	Si	Ca	Mn
FH	+ MG							18	4	17	9	3
FH								6	2	6	4	2
FH	+ MG	+ GT						4	2	1	0	0
FH	+ MG		+ HT					2	1	1	0	0
	MG	+ GT	+ HT					2	1	1	0	0
FH				+ SD				1	0	0	0	0
FH					+ PY			1	1	1	1	0
						MC	+ GR	1	0	0	0	0

[a] FH, ferrihydrite; MG, magnetite; GT, goethite; HT, hematite; SD, siderite; PY, pyrite; MC, mackinawite; GR, greigite.

(*22*). The small (<200 nm long) acicular particles occasionally incorporated in the cryptocrystalline clusters also exhibit lattice fringes of 0.6 nm and are considered to be lepidocrocite.

A high magnification image of one of the cryptocrystalline clusters (Figure 4g) reveals uniformly sized (~5−10 nm), rounded domains. The domains collectively compose cryptocrystalline grains, which become part of the cryptocrystalline clusters. The lattice fringe values found in these domains vary between 0.22 and 0.31 nm (Figure 4h). This image resembles the TEM images of ferrihydrite clusters of both natural and synthetic origins (*20, 25, 26*) in terms of the domain size, variable lattice fringe spacing, and spherical or polyhedral domain habit. It should be noted that the elongated crystal partially shown at the bottom of Figure 4h exhibits the lattice fringe spacing of 0.33 nm. Although the lattice fringe value alone does not suffice for a positive phase identification, this fringe may be lepidocrocite (120).

DFC samples also exhibit cryptocrystalline clusters. They are composed of small (<200 nm) acicular particles and rounded to polyhedral grains (Figure 5). Large (>500 nm) elongated crystals were seldom seen. The SAED patterns from these cryptocrystalline clusters indicate the ubiquitous presence of ferrihydrite, in addition to greigite, magnetite, and occasional mackinawite and goethite (Figure 5b). The SAED-identified phase assemblages for DFC are summarized in Table 3 together with the minor element inventory. The data suggest the strong association between ferrihydrite and metals, as all of the observed clusters contain detectable amounts of Si with associated S and Ca, and occasional Cr.

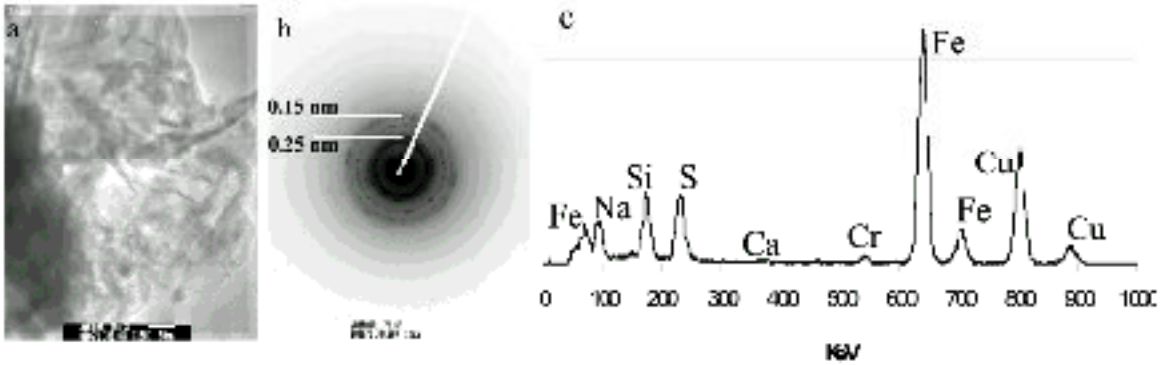

FIGURE 5. (a) TEM bright-field image of a cryptocrystalline cluster from DFC. It is composed of small (<100 nm long) acicular particles and small (<50 nm) rounded to polyhedral particles. (b) SAED image of the cluster shown in (a), exhibiting diffuse ferrihydrite diffraction rings at d = 0.25 and 0.15 nm overlaid with the darker, better defined diffraction rings attributed to mackinawite and greigite. (c) EDX spectrum of the same cluster indicating the presence of Si, Ca and Cr in addition to Fe and S (Cu signals are from the sample holder).

TABLE 3. SAED-Based Phase Assemblages and EDX-Based Minor Element Inventory for DFC Cryptocrystalline Clusters[a]

phase assemblage by SAED				no. of clusters	Si	S	Ca	Cr
FH				4	4	4	3	1
FH	+ MG			3	3	3	1	0
FH		+ GR		3	3	3	3	0
FH			+ GT	1	1	1	1	0
FH		+ GR	+ MC	1	1	1	1	1

[a]FH, ferrihydrite; MG, magnetite; GR, greigite; GT, goethite; MC, mackinawite.

Corrosion Product Paragenesis. The ubiquitous nature of ferrihydrite in EC and DFC samples suggests that the long-term performance of these PRBs may be influenced by the formation and conversion kinetics of ferrihydrite.

A limited number of studies quantitatively discuss the kinetics of ferrihydrite formation and transformation in environments relevant to Fe^0-PRBs. In synthesis studies at ambient temperature, the daylong aeration of dissolved Fe(II) at neutral pH produces lepidocrocite when the solution Si/Fe ratio is < 0.36, and ferrihydrite when it is > 0.36 (*29, 30*). Another synthesis study showed that the hydrolysis of Fe(II) ions in the presence of DIC and subsequent aeration formed ferrihydrite within 60 min through the intermediate steps of carbonate green rust (*27*). Further aeration caused a rapid conversion to more crystalline oxyhydroxides such as lepidocrocite and goethite, but adsorption of phosphate onto ferrihydrite prevented the conversion (*27*). Sorption of other species, including Si and SO_4, has been also reported to stabilize ferrihydrite (*22, 35, 36*). Formation of ferrihydrite as the product of Fe^0 corrosion has also been documented to occur within a few weeks at ambient temperature (*37*). These studies confirm that the observed mineral assemblages in EC and DFC samples are consistent with the Fe mineral paragenesis documented in laboratory studies of iron oxidation: precipitation of ferrihydrite (via carbonate green rust when DIC is present) and subsequent conditional conversion to crystalline iron oxyhydroxides. The conversion to crystalline iron oxyhydroxides is rapid in the absence of adsorbed species. On the other hand, ferrihydrite may persist indefinitely in the presence of stabilizing species such as Si, PO_4 and SO_4. It is worth noting that the EC and DFC groundwaters contain significantly less dissolved Si in the mid-barrier regions than in the upgradient interface regions (Table 1). It is likely that much of dissolved Si is adsorbed to ferrihydrite. The observed association of Si with cryptocrystalline clusters also suggests the adsorption of Si to ferrihydrite.

Carbonate green rust was detected by XRD in materials from EC but was not found by SAED. This may be due to the spatial relationship between Fe^0 surfaces and green rust: green rust may exist either as discrete large particles or as a surface layer on Fe^0 filings that cannot be mechanically separated. The TEM sample preparation technique used in this study permitted a bias toward small particles and clusters. A previous study found that carbonate green rust formed by Fe^0 oxidation is stabilized and conversion to ferrihydrite is retarded if oxygen becomes depleted and phosphate is present (*27*).

Magnetite is another mineral prevailing in both the EC and DFC PRBs. Previous studies showed that the formation of ferrihydrite requires oxygen as an oxidant (*27, 29, 30, 37*). In strictly anaerobic environments, however, the Fe^0 corrosion leads to the final product of magnetite as surface film (*38*). Magnetite is also one of the primary products of microbial ferrihydrite reduction (*39*). The magnetite observed under HRTEM in this study is likely to be the latter because it exists within the discrete clusters together with ferrihydrite rather than as the surface film on Fe^0.

Iron sulfides were also detected by XRD at the upgradient interface of EC (Figure 2) and by SAED from both EC and DFC samples (Tables 2 and 3).

The close proximity of ferrihydrite, lepidocrocite, carbonate green rust, iron sulfides and magnetite thus warrants some combination of three possible explanations: (1) highly active metal reducing bacteria (MRB) and sulfate reducing bacteria (SRB) communities; (2) heterogeneous redox environments supporting simultaneous oxic and anoxic corrosion; and (3) heterogeneous groundwater geochemical regimes in which the concentrations of species that stabilize ferrihydrite and green rust (e.g., Si, PO_4) fluctuate. These explanations are all possible in the study site environments. It has been reported from both EC and DFC that the PLFA structural groups indicative of MRB comprise up to 13% of the total PLFA biomass, whereas those indicative of SRB comprise up to 32% (*9*). Although the bulk groundwater and barrier pore water contain small but detectable concentrations (0.1−0.9 mg/L) of oxygen (Table 1), these data do not exclude the possibility of local anoxia caused by heterogeneity in biogeochemical and hydrological regimes. Thus, the formation of magnetite in these PRBs takes two pathways: anaerobic corrosion of Fe^0 and microbial reduction of ferrihydrite. In anoxic environments, the MRB and SRB communities are likely to take part in iron sulfide formation. Fluctuating sorbate concentrations and oxygen concentrations result in the proximal formation of carbonate green rust, ferrihydrite, and goethite/lepidocrocite. It is interesting to note that lepidocrocite and goethite were seldom seen in DFC samples under TEM. This may be because DFC water

contains larger amounts of TDS than does EC water contributing to the stabilization of ferrihydrite and prevention of lepidocrocite and goethite formation.

The observed mineral assemblages and inferred paragenetic relationship indicate that Fe^0-PRBs maintain complex, non-steady-state transport and reaction regimes. The reaction-transport models with smooth chemical and hydrodynamic gradients (*40*, *41*) have limitations in simulating mineral precipitation in spatially and temporally heterogeneous environments. A stochastic treatment of flow regimes (*42*) combined with stochastic descriptions for the simultaneous precipitations of metastable mineral assemblages may become useful in predicting and evaluating the long term build up of authigenic phases.

Implications for Long-Term Barrier Efficiency. Many PRB applications depend on the reducing nature of Fe^0. Consequently, PRBs must not allow for either complete corrosion of Fe^0 or complete coverage of Fe^0 surfaces by corrosion products.

SEM analysis of EC samples from the upgradient interface indicates that the surfaces of Fe^0 are covered with 10−50 μm thick authigenic precipitates after four years of operation (*3*). The same study showed that the samples further (>8 cm) toward the downgradient end had much thinner (<5 μm) surface precipitates (*3*). Consequently, long-term success of PRB installations requires that the grain size of Fe^0 materials be sufficiently large and the barrier dimension be sufficiently wide along the groundwater flow path. The actual grain sizes and barrier dimensions must be determined according to the chemistry and hydrology of particular sites.

This study revealed ferrihydrite morphology to be discrete globe-shaped clusters (Figures 4 and 5). A previous study has shown that the spatial relationship between Fe^0 surfaces and corrosion products, rather than the overall quantity of corrosion products, determines the reactivity of Fe^0 (*43*). It also showed that the reactivity of Fe^0 surfaces was maintained when Fe^0 corrosion proceeded in high ionic strength water in the presence of oxygen, whereas the reactivity decreased when the corrosion took place in anoxic, low ionic strength water (*43*). It is likely that aerobic, high ionic strength water promotes the formation and stabilization of discrete ferrihydrite clusters away from Fe^0 surfaces, whereas anoxic corrosion promotes the formation of magnetite surface film (*38*) that passivates the Fe^0 surface.

Implications to Other PRB Applications. Ferrihydrite surfaces have very high sorption capacity for many dissolved species including ones with environmental consequences such as Cd^{2+} (*44*−*46*), Pb^{2+}, Cr^{3+} (*33*), AsO_4^{3-} (*47*), and organic compounds present in herbicides (*48*, *49*). In fact, the effectiveness of Fe^0-PRBs for arsenate-contaminated water previously reported is due to sorption rather than reductive precipitation (*43*). The reductive removal of Cr(VI) by Fe^0-PRB may also be enhanced by the sorption of Cr(III) onto ferrihydrite surfaces. Thus, one may take advantage of ferrihydrite formation and stabilization in order to utilize the Fe^0-PRB technology to conduct adsorptive remediation procedures that do not solely rely on redox reactions.

Acknowledgments

The U.S. Environmental Protection Agency through its Office of Research and Development partially funded and collaborated in the research described here under assistance agreement DW17939158 to the Naval Research Laboratory. It has not been subject to Agency review and therefore does not necessarily reflect the views of the Agency, and no official endorsement should be inferred. J.-W.K. was funded by ONRE/NRL Postdoctoral Fellowship. NRL Contribution No. 7430-01-15.

Literature Cited

(1) Puls, R. W.; Blowes, D. W.; Gillham, R. W. *J. Hazard. Mater.* 1999, *68*, 109.
(2) Vogan, J. L.; Focht, R. M.; Clark, D. K.; Graham, S. L. *J. Hazard. Mater.* 1999, *68*, 97.
(3) Blowes, D. W.; Ptacek, C. J.; Jambor, J. L. *Environ. Sci. Technol.* 1997, *31*, 3348.
(4) Puls, R. W.; Paul, C. J.; Powell, R. M. *Appl. Geochem.* 1999, *14*, 989.
(5) Gu, B.; Liang, L.; Dickey, M. J.; Yin, X.; Dai, S. *Environ. Sci. Technol.* 1998, *32*, 3366.
(6) Klausen, J.; Ranke, J.; Schwarzenbach, R. P. *Chemosphere* 2001, *44*, 511.
(7) Gillham, R. W.; O'hannesin, S. F. *Ground Water* 1994, *32*, 958.
(8) Richardson, J. P.; Nicklow, J. W. *Soil. Sediment. Contam.* 2002, *11*, 241.
(9) Wilkin, R. T.; Puls, R. W.; Sewell, G. W. *EPA Environmental Research Brief* 2002; EPA/600/S-02/001.
(10) Roh, Y.; Lee, S. Y.; Elkes, M. P. *Environ. Geol.* 2000, *40*, 184.
(11) Phillips, D. H.; Gu, B.; Watson, D. B.; Roh, Y.; Liang, L.; Lee, S. Y. *Environ. Sci. Technol.* 2000, *34*, 4169.
(12) Mackenzie, P. D.; Horney, D. P.; Sivavec, T. M. *J. Hazard. Mater.* 1999, *68*, 1.
(13) Gu, B.; Phelps, T. J.; Liang, L.; Dickey, M. J.; Roh, Y.; Kinsall, B. L.; Palumbo, A. V.; Jacobs, G. K. *Environ. Sci. Technol.* 1999, *33*, 2170.
(14) Lackovic, J. A.; Nikolaidis, N. P.; Dobbs, G. M. *Environ. Eng. Sci.* 2000, *17*, 29.
(15) Melitas, N.; Wang, J. P.; Conklin, M.; O'Day, P.; Farrell, J. *Environ. Sci. Technol.* 2002, *36*, 2074.
(16) McMahon, P. B.; Dennehy, K. F.; Sandstrom, M. W. *Ground Water* 1999, *37*, 396.
(17) Genin, J. M. R.; Refait, P.; Bourrie, G.; Abdelmoula, M.; Trolard, F. *Appl. Geochem.* 2001, *16*, 559.
(18) Hansen, H. C. B.; Borggaard, O. K.; Sorensen, J. *Geochim. Cosmochim. Acta* 1994, *58*, 2599.
(19) McGill, I. R.; McEnaney, B.; Smith, D. C. *Nature* 1976, *259*, 200.
(20) Janney, D. E.; Cowley, J. M.; Buseck, P. R. *Clays Clay Miner.* 2000, *48*, 111.
(21) Schwertmann, U.; Taylor, R. M. *Clay Miner.* 1979, *14*, 285.
(22) Jambor, J. L.; Dutrizac, J. E. *Chem. Rev.* 1998, *98*, 2549.
(23) Childs, C. W. *Z. Pflanzen. Bodenk.* 1992, *155*, 441.
(24) Parfitt, R. L. *J. Soil Sci.* 1989, *40*, 259.
(25) Taitel-Goldman, N.; Singer, A. *Clays Clay Miner.* 2001, *49*, 174.
(26) Greffie, C.; Amouric, M.; Parron, C. *Clay Miner.* 2001, *36*, 381.
(27) Benali, O.; Abdelmoula, M.; Refait, P.; Genin, J. M. R. *Geochim. Cosmochim. Acta* 2001, *65*, 1715.
(28) Fredrickson, J. K.; Zachara, J. M.; Kennedy, D. W.; Dong, H. L.; Onstott, T. C.; Hinman, N. W.; Li, S. M. *Geochim. Cosmochim. Acta* 1998, *62*, 3239.
(29) Mayer, T. D.; Jarrell, W. M. *Water Res.* 1996, *30*, 1208.
(30) Schwertmann, U.; Carlson, L.; Fechter, H. *Schweizerische Zeitschrift Hydrologie* 1984, *46*, 185.
(31) Bibak, A.; Borggard, O. K. *Soil Sci.* 1994, *158*, 322.
(32) Kinniburgh, D. G. *Environ. Sci. Technol.* 1986, *20*, 895.
(33) Manceau, A.; Charlet, L.; Boisset, M. C.; Didier, B.; Spadini, L.; Meunier, A. 1992, *7*, 201.
(34) Dzombak, D. A.; Morel, F. M. M. *Surface complexation modeling: hydrous ferric oxide*; Wiley: New York, 1990; 393 p.
(35) Carlson, L.; Schwertmann, U. *Geochim. Cosmochim. Acta* 1981, *45*, 421.
(36) Torrent, J.; Guzman, R. *Clay Miner.* *17*, 463.
(37) Abdelmoula, M.; Refait, P.; Drissi, S. H.; Mihe, J. P.; Genin, J. M. R. *Corros. Sci.* 1996, *38*, 623.
(38) Odziemkowski, M. S.; Schuhmacher, T. T.; Gillham, R. W.; Reardon, E. J. *Corros. Sci.* 1998, *40*, 371.
(39) Zachara, J. M.; Kukkadapu, R. K.; Fredrickson, J. K.; Gorby, Y. A.; Smith, S. C. *Geomicrobiol. J.* 2002, *19*, 179.
(40) Mayer, K. U.; Blowes, D. W.; Frind, E. O. *Water Resour. Res.* 2001, *37*, 3091.
(41) Yabusaki, S.; Cantrell, K.; Sass, B.; Steefel, C. *Environ. Sci. Technol.* 2001, *35*, 1493.
(42) Eykholt, G. R.; Elder, C. R.; Benson, C. H. *J. Hazard. Mater.* 1999, *68*, 73.
(43) Farrell, J.; Wang, J. P.; O'Day, P.; Conklin, M. *Environ. Sci. Technol.* 2001, *35*, 2026.
(44) Backes, E. A.; McLaren, R. G.; Rate, A. W.; Swift, R. S. *Soil Sci. Soc. Am. J.* 1995, *59*, 778.

(85) Warren, L. A.; Outridge, P. M.; Zimmerman, A. P. *Hydrobiologia* 1995, *304*, 197.
(86) Spadini, L.; Manceau, A.; Schindler, P. W.; Charlet, L. *J. Colloid Interface Sci.* 1994, *168*, 73.
(87) Langner, H. W.; Inskeep, W. P. *Environ. Sci. Technol.* 2000, *34*, 3131.
(88) Schwandt, H.; Kogelknabner, I.; Stanjek, H.; Totsche, K. *Sci. Total Environ.* 1992, *123*, 121.
(89) Cox, L.; Hermosin, M. C.; Cornejo, J. *Eur. J. Soil Sci.* 1995, *46*, 431.

Received for review January 16, 2002. Revised manuscript received October 16, 2002. Accepted October 16, 2002.

ES025533H